

Near-optimal coherent state discrimination via continuously labelled non-Gaussian measurements

James Moran,^{1,*} Spiros Kechrimparis,^{2,†} and Hyukjoon Kwon^{2,‡}

¹*Quantum Universe Center, Korea Institute for Advanced Study, Seoul 02455, Republic of Korea*

²*School of Computational Sciences, Korea Institute for Advanced Study, Seoul 02455, Republic of Korea*

Quantum state discrimination plays a central role in quantum information and communication. For the discrimination of optical quantum states, the two most widely adopted measurement techniques are photon detection, which produces discrete outcomes, and homodyne detection, which produces continuous outcomes. While various protocols using photon detection have been proposed for optimal and near-optimal discrimination between two coherent states, homodyne detection is known to have higher error rates, with its performance often referred to as the Gaussian limit. In this work, we demonstrate that, despite the fundamental differences between discretely labelled and continuously labelled measurements, continuously labelled non-Gaussian measurements can also achieve near-optimal coherent state discrimination. We explicitly design two coherent state discrimination protocols based on non-Gaussian unitary operations combined with homodyne detection and orthogonal polynomials, which surpass the Gaussian limit. Our results show that photon detection is not required for near-optimal coherent state discrimination and that we can achieve error rates close to the Helstrom bound at low energies with continuously labelled measurements. We also find that our schemes maintain an advantage over the photon detection-based Kennedy receiver for a moderate range of coherent state amplitudes.

I. INTRODUCTION

Quantum state discrimination is a quantum information primitive and is ubiquitous in quantum communications [1–5]. When two quantum states are non-orthogonal, no measurement can perfectly distinguish between them. This fundamental quantum limit is known as the Helstrom bound [6].

In continuous-variable systems, such as quantum optical systems, quantum state discrimination is a fundamental task in optical communications [4, 5]. Due to their experimental availability, robustness to losses, and ease of control, the discrimination of two optical coherent states, also known as binary phase-shift keying (BPSK) [7], is the simplest non-trivial example of optical state discrimination. One issue in continuous-variable systems is that the discrimination task involves determining how to construct an optimal measurement protocol that achieves the Helstrom bound with experimentally feasible technologies. In lieu of Helstrom measurements, which are often challenging to realise, and owing to the non-uniqueness of optimal measurement setups, many receivers designed to discriminate two coherent states have appeared in the literature [8–11]. These receivers are typically based on experiments that can be implemented with current technologies, such as homodyne detection and on-off photon detection. In the literature thus far, only receivers using a final on-off photon detection have been shown to exceed the homodyne limit and, in some cases, reach the Helstrom bound.

It was shown in Ref. [9] that in order to achieve the Helstrom bound for the discrimination of two coherent states, non-Gaussianity is required in the measurement. Specifically, while the optimal performance among Gaussian measurement schemes, known as the *Gaussian limit*, is achieved by homodyne detection—a measurement of a quadrature operator—there remains a gap between this performance and the Helstrom bound. Receivers that are able to achieve the Helstrom bound appeared in Refs. [12, 13] which are now known as the Dolinar and Sasaki-Hirota receivers, respectively. In both cases on-off photon detection, a necessarily non-Gaussian operation is used, and in the Sasaki-Hirota receiver an additional non-Gaussian unitary is applied. This raises the questions: is photon detection necessary to achieve the Helstrom bound in coherent state discrimination? If we are restricted to continuously labelled measurement schemes, such as those based on homodyne or heterodyne detection, can we surpass the Gaussian limit to approach the Helstrom bound? Moreover, what is the form of the non-Gaussian operations that enable us to do this?

In this work, we answer these questions in the affirmative: we define two types of continuously labelled receivers that can exceed the Gaussian limit. The first is constructed from a class of non-Gaussian unitaries which, when combined with homodyne detection, lead to significant performance improvements over the Gaussian limit in both low- and high-energy regimes. The second type is based on the theory of orthogonal polynomials. We find that generalised states based on Legendre and Laguerre polynomials can also exceed the Gaussian limit. This confirms that photon detection is not required for performance beyond the Gaussian limit in coherent state discrimination, and this regime can be achieved with continuously labelled measurements. However, the results do not specify the precise form of non-

* jamesmoran@kias.re.kr

† spiros@kias.re.kr

‡ hjkwon@kias.re.kr

Gaussianity required. We provide examples of continuously labelled non-Gaussian measurement schemes with varying degrees of non-Gaussianity, which are shown to degrade performance below the Gaussian limit.

This paper is structured as follows. In Sec. II we recapitulate the problem of minimum-error quantum state discrimination, the notion of Gaussian and non-Gaussian states and measurements, and the issues that arise when the states to be discriminated belong to infinite-dimensional Hilbert spaces. In Sec. III we introduce the notion of continuously and discretely labelled measurements and analyse their fundamental differences and connection to wave-particle duality. Following this, in Sec. IV we define some continuously labelled receivers based on unitary rotations by pure state projectors and show that they exceed the Gaussian limit. In Sec. V we define a different type of continuously labelled receiver, based on the orthogonality of the Legendre polynomials, and show that this receiver also exceeds the Gaussian limit. In Sec. VI we discuss the role of non-Gaussianity in coherent state discrimination. Based on the stellar rank, we find two examples at finite and infinite non-Gaussianity which are detrimental to the error rate, showing that non-Gaussianity does not guarantee improved discrimination performance. Lastly, in Sec. VII, we conclude by summarising our findings and addressing future directions this work could take.

II. COHERENT STATE DISCRIMINATION

A. Minimum-error discrimination

Minimum-error discrimination of two states, $\hat{\rho}_1, \hat{\rho}_2$, with prior probabilities, $p_1, p_2 = 1 - p_1$, respectively, is characterised by a two-element positive operator-valued measure (POVM), $\{\hat{\Pi}_1, \hat{\Pi}_2 = \mathbb{I} - \hat{\Pi}_1\}$, where $\hat{\Pi}_i$ corresponds to the hypothesis, \mathcal{H}_i , that guesses the state's label as i . For non-orthogonal quantum states there is a non-zero error in determining which state was sent. Concretely, the probability of error, P_E , is given by the following Bayes' probability law [1, 2]

$$P_E = p_1 \text{tr} [\hat{\Pi}_2 \hat{\rho}_1] + p_2 \text{tr} [\hat{\Pi}_1 \hat{\rho}_2]. \quad (1)$$

The minimisation of Eq. (1), with respect to $\hat{\Pi}_i$, leads to the Helstrom bound [6], which describes the fundamental quantum limit on the minimum-error discrimination of two non-orthogonal quantum states. The Helstrom bound is given by

$$P_H = \frac{1}{2} (1 - \text{tr} \|p_2 \hat{\rho}_2 - p_1 \hat{\rho}_1\|_1), \quad (2)$$

where $\|\hat{O}\|_1 = \text{tr} [\sqrt{\hat{O}^\dagger \hat{O}}]$ denotes the trace-norm.

In this work we will restrict our attention to the case of two pure states, $\hat{\rho}_i = |\psi_i\rangle\langle\psi_i|$, and equal prior probabilities, $p_1 = p_2 = \frac{1}{2}$. The Helstrom bound Eq. (2)

becomes

$$P_H = \frac{1}{2} \left(1 - \sqrt{1 - |\langle\psi_1|\psi_2\rangle|^2} \right), \quad (3)$$

and the optimal measurements obtained from the theory are projections onto the positive and negative eigenspaces of the operator $\delta\hat{\rho} = \hat{\rho}_1 - \hat{\rho}_2$.

B. Coherent states and Gaussian measurements

States which are ubiquitous to quantum optics are the Glauber-Sudarshan coherent states [14, 15]. Coherent states are considered the most classical amongst quantum states because they minimise the Heisenberg uncertainty principle and their semiclassical equations of motion exactly mimic the equations of motion for classical oscillators. The coherent states have the following Fock state expansion,

$$|\alpha\rangle = e^{-\frac{|\alpha|^2}{2}} \sum_{n=0}^{\infty} \frac{\alpha^n}{\sqrt{n!}} |n\rangle, \quad \alpha \in \mathbb{C}. \quad (4)$$

The coherent states may also be represented by a complex displacement of the vacuum state in phase space by the displacement operator

$$\hat{D}(\alpha) = \exp(\alpha\hat{a}^\dagger - \bar{\alpha}\hat{a}), \quad (5)$$

such that $|\alpha\rangle = \hat{D}(\alpha)|0\rangle$. Coherent states are referred to as *Gaussian states* because their Wigner phase space distributions are Gaussian [16]. Gaussian operations are then defined as operations that transform Gaussian states to Gaussian states, and Gaussian unitaries may be formed by the evolution of Hamiltonians which are at most quadratic in the creation and annihilation operators [16–18].

This also underpins the framework for Gaussian measurements. Gaussian measurements are described by the following POVM elements [16, 19]

$$d^2\beta \hat{\Pi}_G(\beta) = d^2\beta \frac{1}{\pi} \hat{D}(\beta) \hat{\rho}_G \hat{D}^\dagger(\beta), \quad (6)$$

satisfying the normalisation condition

$$\int_{\beta \in \mathbb{C}} d^2\beta \hat{\Pi}_G(\beta) = \mathbb{I}. \quad (7)$$

Here $\hat{\rho}_G$ is a zero-mean Gaussian state. A Gaussian state is fully characterised by its covariance matrix and a coherent displacement vector and a zero-mean Gaussian state is a Gaussian state whose displacement vector is zero. In this setting, a two-outcome POVM as described in Sec. II A would be defined by splitting the integration region (7) into two distinct regions, $\mathcal{R}_1, \mathcal{R}_2$, satisfying $\mathcal{R}_1 \cup \mathcal{R}_2 = \mathbb{C}$ and $\mathcal{R}_1 \cap \mathcal{R}_2 = \emptyset$, with the additional requirement that both \mathcal{R}_1 and \mathcal{R}_2 have non-zero

Lebesgue measure. Gaussian measurements include measurement of quadrature eigenstates (i.e. homodyne detection), which may be interpreted through (6) as a measurement of infinitely squeezed coherent states, and heterodyne detection (i.e. projections onto coherent states) [20, 21].

An identity related to the total variation distance of two probability distributions which will come in useful for the analysis that follows is the following [22]

$$P_E = \frac{1}{2} - \frac{1}{4} \int_{x \in \mathcal{X}} dx |\rho_1(x) - \rho_2(x)|, \quad (8)$$

where $\rho_i(x) = \text{tr} [\hat{\Pi}_x \hat{\rho}_i]$ is the continuous probability distribution induced by the POVM, $\{\hat{\Pi}_x\}$. This formula is useful because we can replace the integration over a to-be-determined region, \mathcal{R}_2 (the region where $(\rho_1(x) - \rho_2(x))$ is negative), by an integration of the absolute value of the difference between the distributions over the entire real line.

C. Coherent state discrimination

Applying the theory of minimum-error discrimination to two coherent states with opposite signs in their amplitudes, $\{|\alpha\rangle, |-\alpha\rangle\}$, $\alpha \in \mathbb{R}$, yields an optimal measurement of the form [6]

$$\hat{\Pi}_2 = |-\rangle \langle -|, \quad (9)$$

where

$$\begin{aligned} |-\rangle = & \left(\frac{1 - \sqrt{1 - e^{-4\alpha^2}}}{\sqrt{1 - e^{-4\alpha^2}}} \right) |\alpha\rangle \\ & + \left(2e^{-2\alpha^2} - \frac{e^{-2\alpha^2}}{\sqrt{1 - e^{-4\alpha^2}}} \right) |-\alpha\rangle, \end{aligned} \quad (10)$$

and $\hat{\Pi}_1 = |+\rangle \langle +| = \mathbb{I} - |-\rangle \langle -|$, with the identity operator here being valid on the signal space, $\mathbb{I}|\pm\alpha\rangle = |\pm\alpha\rangle$.

The optimal measurement in state discrimination problems is not unique [1, 2]. Moreover, the actual implementation of the Helstrom measurement of the form of Eq. (9) is a projection onto a cat state, and is impractical with today's technologies. Only recently have projective measurements onto cat state bases been performed [23], but this is only in the low-amplitude limit and it is achieved with poor fidelity due to detector imperfections. The Dolinar principle has been demonstrated experimentally [24], but continuous feedback techniques come with several drawbacks, including low symbol repetition rate and the need for fast detectors. With these limitations in mind, various optical receivers designed to approach and in some cases saturate the Helstrom bound for BPSK have been conceived.

The Helstrom bound for BPSK is

$$P_E^{\text{Helstrom}} = \frac{1}{2} \left(1 - \sqrt{1 - e^{-4\alpha^2}} \right), \quad (11)$$

while the limit when restricted to Gaussian measurement schemes is given by [9]

$$P_E^G = \frac{1}{2} \left(1 - \text{erf} \left(\sqrt{2}|\alpha| \right) \right), \quad (12)$$

and the Gaussian limit is achieved by homodyne detection. We see that there is a significant gap between these two functions at finite non-zero α . This exposes the importance of quantum measurements in state discrimination scenarios, if we are able to go beyond the Gaussian limit we can see potentially exponential improvements in error rates.

From here on we will refer to any receiver whose performance lies strictly between the Gaussian limit and the Helstrom bound for any range of $|\alpha|^2$ as *near-optimal*, and any receiver which performs worse than the Gaussian limit, despite invoking non-Gaussian operations, we will refer to as *non-optimal*.

Given that the Helstrom measurement, Eq. (9), may be implemented through photon detection [13], all optimal and near-optimal receivers in the literature make use of photon detection (14) to exceed the Gaussian limit. The most notable examples include the near-optimal Kennedy receiver [25] which uses displacement followed by on-off photon detection. The measurement setup is as follows

$$\hat{\Pi}_1 = \hat{D}^\dagger(\alpha) \hat{\Pi}_{\text{off}} \hat{D}(\alpha), \quad \hat{\Pi}_2 = \hat{D}^\dagger(\alpha) \hat{\Pi}_{\text{on}} \hat{D}(\alpha), \quad (13)$$

where

$$\hat{\Pi}_{\text{off}} = |0\rangle \langle 0|, \quad \hat{\Pi}_{\text{on}} = \sum_{n=1}^{\infty} |n\rangle \langle n|. \quad (14)$$

The principle idea is to displace the alphabet $\{|\alpha\rangle, |-\alpha\rangle\} \rightarrow \{|0\rangle, |2\alpha\rangle\}$ and then perform on-off detection where a measurement outcome of 'on' would indicate that the state is $|2\alpha\rangle$, and an outcome of 'off' would be ambiguous, but there is higher probability that it is the state $|0\rangle$. In the high-energy regime the Kennedy receiver gives lower error rates than the Gaussian limit, but there remains an exponential gap with the Helstrom bound.

The first optimal receiver to appear in the literature was the Dolinar receiver [12]. The Dolinar receiver expands on the Kennedy receiver by including real-time feedback such that the displacement parameter in (13) is dynamically updated according to the intermediate measurement outcomes. The Dolinar receiver was also shown to be robust in the presence of noise [26], and it may be interpreted as a multiple-copy discrimination problem [27].

The Sasaki-Hirota receiver was also shown to be optimal for BPSK and it simplifies the need for a complex feedback mechanism at the expense of requiring a non-Gaussian unitary rotation onto a cat state as a preprocessing, followed by on-off photon detection. Unlike the

Dolinar receiver, the Sasaki-Hirota receiver was shown to not be robust in the presence of noise.

A variety of other near-optimal receivers have appeared in the literature for BPSK and similar problems [7, 28, 29], usually based on operations that are realistically implementable with current technologies. In all optimal and near-optimal receivers in the literature, photon detection is used. Given that no near-optimal schemes based on continuously labelled measurements exist in the literature, we will investigate this in the following.

III. CONTINUOUSLY AND DISCRETELY LABELLED MEASUREMENTS

Homodyne detection and photon detection represent measurements of fundamentally different properties of a quantum system, which correspond to wave-like and particle-like properties, respectively. The phenomenon of quantum systems exhibiting both wave-like and particle-like behavior is known as wave-particle duality [30, 31]. In the problem we are exploring in this paper, the wave-particle duality manifests itself as the fundamental inequivalence between measurements with continuous and discrete spectra, corresponding to wave-like and particle-like properties, respectively. For a review on discrete- and continuous-variable quantum information, we refer the reader to [32].

To see this inequivalence explicitly, we show that continuously labelled measurements cannot reproduce on-off photon counting in Eq. (14). Consider the following family of continuously labelled operators, $|\psi\rangle\langle\psi|$ satisfying a completeness relation,

$$\int_{\psi \in \mathcal{X}} d\psi \mu(\psi) |\psi\rangle\langle\psi| = \sum_{n=0}^{\infty} |n\rangle\langle n| = \mathbb{I}, \quad (15)$$

for some positive integral measure $\mu(\psi)$ on some uncountably infinite set \mathcal{X} . If on-off detection were possible by a measurement on ψ , then there should exist a region $\mathcal{Y} \subset \mathcal{X}$, with \mathcal{Y} being dense \mathcal{X} , such that

$$\int_{\psi \in \mathcal{Y}} d\psi \mu(\psi) |\psi\rangle\langle\psi| = \hat{\Pi}_{\text{off}}. \quad (16)$$

Expanding $|\psi\rangle$ in the number basis,

$$|\psi\rangle = \sum_{n=0}^{\infty} c_n(\psi) |n\rangle, \quad (17)$$

where we need not impose any normalisation restriction on the coefficients $c_n(\psi)$, so that this setup accounts for measurements like homodyne detection. However, we observe that $\forall n$ there must exist some range of $\psi \in \mathcal{Z}_n$ where

$$\mathcal{Z}_n = \{\psi \in \mathcal{X} \mid c_n(\psi) \neq 0\}, \quad (18)$$

with $\mathcal{Z}_n \subseteq \mathcal{X}$, dense in \mathcal{X} . This condition follows from the requirement that we have non-zero projectors onto

every number state in (15) and as such every coefficient $c_n(\psi)$ must be non-zero at least somewhere in \mathcal{X} . Moreover, we get the following integral identities for the expansion coefficients

$$\int_{\psi \in \mathcal{X}} d\psi \mu(\psi) c_n(\psi) \bar{c}_m(\psi) = \delta_{nm}, \quad \forall n, m. \quad (19)$$

Expanding (16) in the number basis we get the following matrix elements

$$\mathcal{I}_{nm} = \int_{\psi \in \mathcal{Y}} d\psi \mu(\psi) c_n(\psi) \bar{c}_m(\psi) |n\rangle\langle m|, \quad (20)$$

and in particular we focus on the diagonal elements

$$\mathcal{I}_{nn} = \int_{\psi \in \mathcal{Y}} d\psi \mu(\psi) |c_n(\psi)|^2 |n\rangle\langle n|. \quad (21)$$

Due to the fact that the coefficients $|c_n(\psi)|^2$ are positive for every n and ψ , we thus have the following,

$$0 \leq \langle n | \mathcal{I}_{nn} | n \rangle \leq 1, \quad (22)$$

with the upper bound being saturated only for $\mathcal{Y} = \mathcal{X}$. The implication of this is that the only way to achieve exact projection onto the ground state is by taking the set $\mathcal{Y} = \mathcal{X}$, but this of course does not realise photon-counting as we have projections onto all diagonal states with coefficient 1, i.e., we have reproduced the identity operator (15). Thus there is no way to exactly reproduce on-off photon counting by a continuously labelled measurement. This is shown explicitly for the examples of heterodyne and homodyne detection in App A. We remark that we are talking about equivalence in the strict sense (i.e. an equality), one may attempt to construct a continuously labelled measurement, which up to an error can reproduce a vacuum state projection, but we exclude such examples in the present work. We are also excluding reconstructions of photon-number statistics through phase-averaged homodyne measurements [33], as we are focusing on single-shot measurement schemes.

Another important remark is that photon-counting is *always* non-Gaussian, while certain types of continuously labelled non-Gaussian measurements may be interpreted as Gaussian measurement of a non-Gaussian-transformed state. These examples include preprocessing by non-Gaussian unitaries followed by homodyne detection. We may interpret this as a homodyne (Gaussian) detection of a preprocessed non-Gaussian state. We will consider examples of this in the following.

IV. NON-GAUSSIAN UNITARIES COMBINED WITH HOMODYNE MEASUREMENT

Given that homodyne detection defines the Gaussian limit, we look for non-Gaussian unitary operations, \hat{U}_{NG} ,

and construct the following continuously labelled POVM elements

$$dx \hat{U}_{\text{NG}}^\dagger |x\rangle \langle x| \hat{U}_{\text{NG}}. \quad (23)$$

In our setup, this amounts to a preprocessing our coherent states by

$$|\pm\alpha\rangle \rightarrow \hat{U}_{\text{NG}} |\pm\alpha\rangle, \quad (24)$$

and then performing homodyne detection on resulting non-Gaussian states. Given this, we look for non-Gaussian unitaries which can reduce the overlap between $|\alpha\rangle$ and $|\alpha\rangle$, and thus reduce error rates in their discrimination

A. Unitary rotations by pure state projectors

As a special instance of non-Gaussian unitary operations, we consider the following

$$\hat{U}_{\{|\psi_k\rangle\}}^{(N)}(\vec{\theta}) = \prod_{k=0}^N \exp[-i\theta_k |\psi_k\rangle \langle \psi_k|], \quad (25)$$

where $\vec{\theta} = (\theta_0, \theta_1, \dots, \theta_N)$ is an $(N+1)$ -dimensional vector. With the correct choice of states, $\{|\psi_k\rangle\}$, such unitary rotations allow for near-optimal coherent state discrimination. When combined with a homodyne detector, the final POVM elements are given by

$$dx \hat{\Pi}_{\{|\psi_k\rangle\}}^{(N)}(\vec{\theta}) = dx \left[\hat{U}_{\{|\psi_k\rangle\}}^{(N)}(\vec{\theta})^\dagger |x\rangle \langle x| \hat{U}_{\{|\psi_k\rangle\}}^{(N)}(\vec{\theta}) \right]. \quad (26)$$

The action of these unitary operations on an arbitrary input state is

$$\hat{U}_{\{|\psi_k\rangle\}}^{(N)}(\vec{\theta}) |\Psi\rangle = |\Psi\rangle + \sum_{k=0}^N \left(\sum_{\sigma \in \mathcal{T}} \prod_{j=0}^k \zeta_{\sigma(j)} \right) |\Psi\rangle, \quad (27)$$

where

$$\begin{aligned} \sigma \in \mathcal{T} &\iff \{\sigma : \{0, \dots, k\} \rightarrow \{0, \dots, N\} \text{ is injective} \\ &\wedge \{k < N \implies \sigma(k) < \sigma(k+1)\}\}, \end{aligned} \quad (28)$$

with $|\mathcal{T}| = \binom{N+1}{k+1}$ and

$$\zeta_k = (e^{-i\theta_k} - 1) |\psi_k\rangle \langle \psi_k|. \quad (29)$$

The set \mathcal{T} ensures that all the products of terms appear in the correctly indexed order given the fact that the terms inside Eq. (25) in general do not commute. When the states $\{|\psi_k\rangle\}$ are all orthogonal, Eq. (27) simplifies to

$$\hat{U}_{\{|\psi_k\rangle\}}^{(N)}(\vec{\theta}) |\Psi\rangle = |\Psi\rangle + \sum_{k=0}^N (e^{-i\theta_k} - 1) \langle \psi_k | \Psi \rangle |\psi_k\rangle. \quad (30)$$

The optimal choice of the parameters $\vec{\theta}$ will depend on the input state. As we want to discriminate two coherent states, $\{|\alpha\rangle, |-\alpha\rangle\}$, these optimal parameters will in general implicitly depend on the intensity $|\alpha|^2$. It is worth remarking that while the states we rotate by, $\{|\psi_k\rangle\}$ may be Gaussian, the unitary rotation is generally not.

If we let $N = 0$ such that we rotate by one state, the optimal rotation angle can be determined exactly, this is because if any improvement is obtained in any region by such a rotation, it is scaled by a factor proportional to $(1 - \cos \theta_0)$, which is maximised at $\theta_0 = \pi$. To see this, consider rotation of a real coherent state, $|\pm\alpha\rangle$, by a state $|\psi\rangle$ with a real-valued wavefunction (which are the examples we will consider in the subsequent sections), we find the following probability density

$$\begin{aligned} & \left| \langle x | \hat{U}_{\{|\psi\rangle\}}^{(0)}(\vec{\theta}) |\alpha\rangle \right|^2 = |\langle x | \alpha \rangle|^2 \\ & + 2(1 - \cos \theta) \left(|\langle \psi | \alpha \rangle|^2 |\langle x | \psi \rangle|^2 - \langle x | \alpha \rangle \langle \psi | \alpha \rangle \langle x | \psi \rangle \right) \\ & = |\langle x | \alpha \rangle|^2 + 2(1 - \cos \theta) \mathcal{F}(x, \alpha, \psi), \end{aligned} \quad (31)$$

where we have defined the quantity

$$\mathcal{F}(x, \alpha, \psi) = |\langle \psi | \alpha \rangle|^2 |\langle x | \psi \rangle|^2 - \langle x | \alpha \rangle \langle \psi | \alpha \rangle \langle x | \psi \rangle. \quad (32)$$

When we compute the error rate, P_E , we find

$$\begin{aligned} P_E &= \frac{1}{2} + \frac{1}{2} \int_{x \in \mathcal{R}_2} dx \left(|\langle x | \alpha \rangle|^2 - |\langle x | -\alpha \rangle|^2 \right) \\ & + (1 - \cos \theta) \int_{x \in \mathcal{R}_2} dx (\mathcal{F}(x, \alpha, \psi) - \mathcal{F}(x, -\alpha, \psi)), \end{aligned} \quad (33)$$

where the top line of (33) must be upper bounded by the homodyne limit, P_E^G , and if a non-Gaussian enhancement in the error rate occurs, it must then occur in the second line, which will always be optimised by $\theta = \pi$. If we consider $N > 0$, the optimal rotation angles will in general change. For more details on increasing N , see App. B.

In the following subsections we will consider different sets of states $\{|\psi_k\rangle\}$, typical to quantum optics, and see POVMs of the form (26) show non-Gaussian advantage over homodyne detection, with homodyne detection being recovered when $\vec{\theta} = \vec{0}$.

B. Unitary cat state rotations

Motivated by the appearance of cat states in the optimal measurements in Eq. (9), we observe that we can generate cat states by an appropriate choice of states in Eq. (30). Consider the following

$$\{|\psi_k\rangle\} = \{|\text{cat}(\beta_k, \varphi_k)\rangle\}, \quad (34)$$

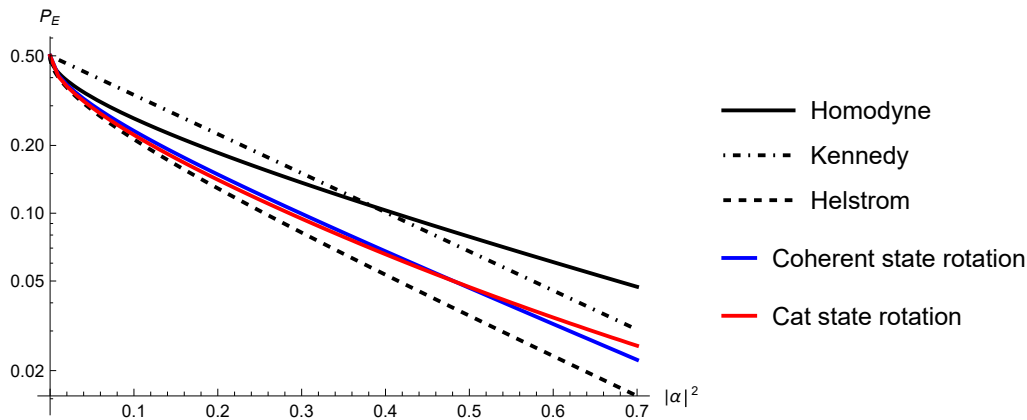


FIG. 1. Comparison of the two best performing near-optimal continuously labelled receivers in Tab. I versus the homodyne, Kennedy and Helstrom limits in the energy range $0 < |\alpha|^2 < 0.7$. Here we find that the cat state rotation and coherent state rotation perform best

where a general two-headed cat state is given by

$$|\text{cat}(\beta, \varphi)\rangle = \frac{1}{\sqrt{2(1 + e^{-2|\beta|^2} \cos \varphi)}} (|\beta\rangle + e^{i\varphi} |-\beta\rangle). \quad (35)$$

We let $N = 0$, such that we just rotate by one even cat state (i.e. we take $\varphi = 0$) and take $\vec{\theta} = (\pi)$. This generates a three-headed cat state by Eq. (30). In the energy regime $0 < |\alpha|^2 < 0.47$, we find a significant advantage over a homodyne receiver, the Kennedy receiver, and other near-optimal receivers considered listed in Tab. I. In the high-energy regime the performance of the cat state rotation falls off, though it maintains an advantage over homodyne detection. The performance of the cat states is plotted in Fig. 1. For details on the optimal scaling of the cat state parameter, β , see App. C.

C. Unitary coherent state rotations

Next we consider rotating by coherent states,

$$\{|\psi_k\rangle\} = \{|\beta_k\rangle\}, \quad (36)$$

by Eq. (30), this will generate a two-headed cat state. Again, letting $N = 0$ and taking the optimal rotation angle $\vec{\theta} = (\pi)$, when applied to our input coherent states $|\pm\alpha\rangle$ this effectively generates another cat state which we then discriminate via homodyne detection. In the low-energy regime, we find performance improvements commensurable with the Fock state rotations. The improvements aren't as sharp in the very low-energy regime as the cat state rotations, but the improvement is more stable over a larger range of energies.

We plot the performance of the coherent state rotation-based receiver in Figs. 1 and 2. In the low-energy regime ($0 < |\alpha|^2 < 0.47$) the coherent state rotation-based receiver is narrowly beaten by the cat state rotation. At around $|\alpha|^2 = 1.4$ the coherent state rotation is beaten by

the Kennedy receiver. For details on the optimal scaling of the coherent state parameter, β , see App. C.

V. CONTINUOUSLY LABELLED NON-GAUSSIAN MEASUREMENTS BASED ON ORTHOGONAL POLYNOMIALS

Another way to construct a continuously labelled POVM is to use families of orthogonal polynomials. One way to view the completeness relation of the quadrature eigenstates is by the completeness relation of the Hermite polynomials. Just as the quadrature eigenstates are not themselves normalisable and as such are not proper quantum states, we also won't require this for the construction of generalised states for measurement purposes. Explicitly, we may view the quadrature eigenstates in the Fock basis as

$$|x\rangle = \frac{e^{-\frac{x^2}{2}}}{\pi^{\frac{1}{4}}} \sum_{n=0}^{\infty} \frac{1}{\sqrt{2^n n!}} H_n(x) |n\rangle, \quad (37)$$

with a completeness relation derived from the orthogonality of the Hermite polynomials,

$$\frac{1}{\sqrt{\pi} 2^n n!} \int_{x \in \mathbb{R}} dx e^{-x^2} H_n(x) H_m(x) = \delta_{nm}. \quad (38)$$

We may consider other classes of orthogonal polynomials satisfying these conditions and construct quantum measurements from them.

To this end, consider the following Fock expansion based on the Legendre polynomials

$$|s\rangle = \sum_{n=0}^{\infty} \sqrt{\frac{(2n+1)}{2}} P_n(s) |n\rangle, \quad (39)$$

where the Legendre polynomials, $P_n(s)$, have the explicit form

$$P_n(s) = \sum_{m=0}^n \binom{n}{m} \binom{n+m}{m} \left(\frac{s-1}{2}\right)^m. \quad (40)$$

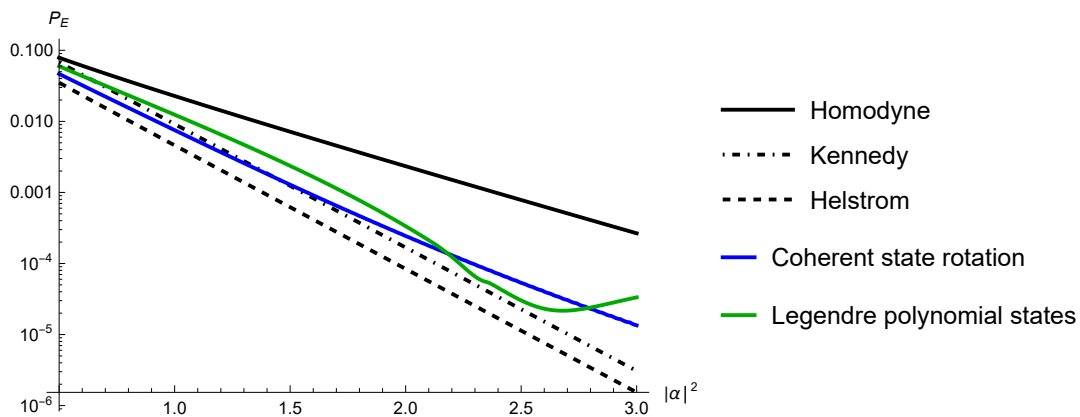


FIG. 2. Comparison of the two best performing near-optimal continuously labelled receivers in Tab. I versus the homodyne, Kennedy and Helstrom limits in the energy range $0.5 < |\alpha|^2 < 3$. Here we find that the coherent state rotation and Legendre states perform best

The argument of the Legendre polynomial satisfies $s \in [-1, 1]$ and owing to their orthogonality relations, the states (39) satisfy the completeness relation

$$\int_{-1}^1 ds |s\rangle \langle s| = \sum_{n=0}^{\infty} |n\rangle \langle n| = \mathbb{I}. \quad (41)$$

We plot the performance of the Legendre states in Fig. 2. We find a substantial improvement over homodyne detection, and, moreover, of all the receivers we consider in this paper we found the second-largest improvement in the high-energy limit using the Legendre states. In the energy region around $2.2 < |\alpha|^2 < 2.7$ the Legendre polynomial states surpass the coherent state rotations and approach the Kennedy receiver limit. Beyond this region the performance deteriorates.

For more details on using orthogonal polynomials to construct POVMs, we direct the reader to App. D.

VI. NON-OPTIMAL CONTINUOUSLY LABELLED NON-GAUSSIAN MEASUREMENTS

Though we know that non-Gaussianity is required for near-optimal discrimination of coherent states, we do not in general have a quantification for how much is required, nor a precise form. Moreover, non-Gaussianity is not *always* helpful in state discrimination.

To see this we must consider some measure of quantum non-Gaussianity. Several quantifications of quantum non-Gaussianity of quantum states have appeared in the literature. These include: the Wigner function negativity [34], the quantum relative entropy [35], and robustness measures [36]. The measure we will use is the recently introduced stellar rank [37], a measure which may be interpreted as the number of photon-additions needed to be applied to a reference Gaussian state. This interpretation provides a natural taxonomy of non-Gaussian states by partitioning the infinite-dimensional Hilbert space of states into classes with the same stellar rank.

For a pure state in an infinite-dimensional Hilbert space the stellar function is defined by

$$F_{\psi}^*(\alpha) = e^{\frac{1}{2}|\alpha|^2} \langle \alpha^* | \psi \rangle = \sum_{n \geq 0} \psi_n \frac{\alpha^n}{\sqrt{n!}}, \quad \forall \alpha \in \mathbb{C}. \quad (42)$$

The stellar rank, $r^*(\psi)$, is equal to the number of zeroes in the function $F_{\psi}^*(\alpha)$. For our purposes, we are interested in characterising non-Gaussian measurements, to which end we use the convex roof construction for mixed states,

$$\hat{\rho} = \int d\gamma p(\gamma) |\psi(\gamma)\rangle \langle \psi(\gamma)|, \quad (43)$$

$$r^*(\hat{\rho}) = \inf_{\{p(\gamma), |\psi(\gamma)\rangle\}} \sup_{\gamma} \{r^*(\psi(\gamma))\},$$

and we will extend this definition to POVM elements. As we are dealing with binary POVMs, we will take the maximum stellar rank between the two elements. In other words for a POVM, $\{\hat{\Pi}_1, \hat{\Pi}_2\}$, we define the following,

$$r_{\max}^*(\hat{\Pi}) = \max \left\{ r^*(\hat{\Pi}_1), r^*(\hat{\Pi}_2) \right\}. \quad (44)$$

By the extension in (44) we find that homodyne and heterodyne have stellar rank $r^*(\hat{\Pi}) = 0$, as expected, while on-off photon detection has stellar rank $r^*(\hat{\Pi}) = \infty$. This exposes one of the essential differences between continuously and discretely labelled measurements. For continuously labelled measurements we strictly have $r^*(\hat{\Pi}_1) = r^*(\hat{\Pi}_2)$ and both elements always have infinite rank (in the functional analysis sense), while for discretely labelled measurements these properties may not be true. More details can be found in App. E.

Proceeding with definition (44) we examine the non-Gaussian resources needed for near-optimal coherent state discrimination. All known optimal receivers, have

TABLE I. A summary of the continuously labelled measurement schemes studied in this paper, their POVM elements, and the maximum stellar rank (44) of the binary POVM. Of the measurements considered, we found improvement over the Gaussian limit by the generalised states based on the Legendre polynomials (39) and Laguerre (see App. D), as well as the unitary rotations followed by homodyne detection, described in (26). Here $|x\rangle, x \in \mathbb{R}$ refers to a quadrature eigenstate, $|\beta\rangle, \beta \in \mathbb{C}$, a coherent state, $|n\rangle, n \in \mathbb{N}$, a Fock state, $|s\rangle, s \in [-1, 1]$, a Legendre polynomial state, and $|r; \nu\rangle, r \in [0, \infty), \nu \in [-1, \infty)$, a Laguerre polynomial state.

Continuously labelled measurement	POVM elements, $\hat{\Pi}$	Stellar rank, $r_{\max}^*(\hat{\Pi})$	Near-optimal?
Homodyne	$dx x\rangle \langle x $	0	No
Heterodyne	$d^2\beta \frac{1}{\pi} \beta\rangle \langle \beta $	0	No
Photon-added coherent states	$d^2\beta \frac{1}{\pi} \hat{D}^\dagger(\beta) n\rangle \langle n \hat{D}(\beta)$	n	No
Cubic phase gate + homodyne	$dx e^{-i\gamma \hat{p}^3} x\rangle \langle x e^{i\gamma \hat{p}^3}$	∞	No
Unitary Fock state rotation + homodyne	$dx \left[\hat{U}_{\{\{k\}\}}^{(N)}(\vec{\theta}) \right]^\dagger x\rangle \langle x \hat{U}_{\{\{k\}\}}^{(N)}(\vec{\theta})$	∞	Yes
Unitary cat state rotation + homodyne	$dx \left[\hat{U}_{\{\{\text{cat}_k\}\}}^{(N)}(\vec{\theta}) \right]^\dagger x\rangle \langle x \hat{U}_{\{\{\text{cat}_k\}\}}^{(N)}(\vec{\theta})$	∞	Yes
Unitary coherent state rotation + homodyne	$dx \left[\hat{U}_{\{\{\beta_k\}\}}^{(N)}(\vec{\theta}) \right]^\dagger x\rangle \langle x \hat{U}_{\{\{\beta_k\}\}}^{(N)}(\vec{\theta})$	∞	Yes
Generalised Laguerre polynomial states	$dr r; \nu\rangle \langle r; \nu $	≥ 1	Yes
Legendre polynomial states	$ds s\rangle \langle s $	≥ 1	Yes

infinite stellar rank because they are based on on-off photon detection. For continuously labelled measurements, the results are summarised in Tab. I. We find that the receivers based on unitary non-Gaussian rotations all had infinite stellar rank (Eq. (26)), while the receivers based on orthogonal polynomials (Eq. (41)) have non-zero stellar rank, but precise determination of the zeroes of their stellar functions is difficult (see App. D).

A. Photon-added coherent states

To see that non-Gaussianity is not always useful, consider the n -photon-added coherent states (n-PACS). The n-PACS are defined as follows [38, 39]

$$|\beta; n\rangle = \hat{D}(\beta) |n\rangle, \quad (45)$$

and, owing to their completeness relations (see App. E), we may construct the following POVM elements

$$d^2\beta \hat{\Pi}_{\beta; n} = d^2\beta \frac{1}{\pi} \hat{D}^\dagger(\beta) |n\rangle \langle n| \hat{D}(\beta). \quad (46)$$

For finite n , these have finite stellar rank $r^*(\hat{\Pi}_{\beta; n}) = n$. They also closely resemble the Kennedy receiver. The only difference being that we resolve the identity over the phase-space variable β , and not over the occupation number n . Despite this, measurements with n-PACS perform worse than the Gaussian limit. Moreover, the performance degrades with increasing n for all values of n that we tested. This behaviour is shown in Fig. 3 where we compare homodyne detection and n-PACS with 1 and 2 photons added.

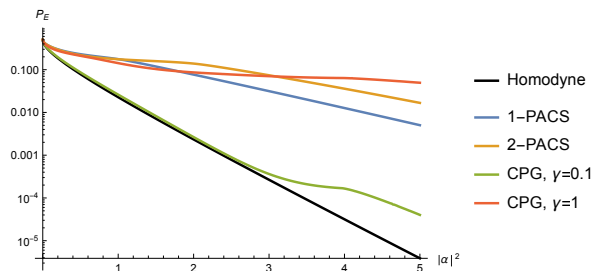


FIG. 3. Performance of the PACS-based receivers $\hat{\Pi}_{\beta; 1}$ and $\hat{\Pi}_{\beta; 2}$, and CPG-based receivers for $\gamma = 0.1$ and $\gamma = 1$ versus homodyne detection.

B. Cubic phase gate

Infinite stellar rank also does not ensure near-optimal performance in coherent state discrimination. To see this, consider the cubic phase gate (CPG). The CPG is the canonical non-Gaussian element in optical quantum computing [40]. It represents the lowest-order non-Gaussian element (or gate in computing nomenclature) which when added to the Gaussian gate set can enable universal optical quantum computing. Despite the difficulties in its experimental realisation [41–43], the utility of the CPG remains an active area of research both theoretically and practically.

In the present context, we are interested in its utility in BPSK. The CPG is given by

$$\hat{U}(\gamma) = e^{i\gamma \hat{p}^3}, \quad \gamma \in \mathbb{R}, \quad (47)$$

where \hat{p} is the momentum operator. Applying this to a coherent state and taking the position space wavefunc-

tion we find

$$\langle x | e^{i\gamma\hat{p}^3} | \alpha \rangle = \frac{(4\pi)^{\frac{1}{4}}}{|3\gamma|^{\frac{1}{3}}} e^{\frac{1}{108\gamma^2}} e^{\frac{x-\sqrt{2}\alpha}{6\gamma}} \text{Ai} \left((3\gamma)^{-\frac{1}{3}} \left(x - \sqrt{2}\alpha + \frac{1}{12\gamma} \right) \right). \quad (48)$$

Here $\text{Ai}(x)$ is the Airy function of the first kind [44]. Note that typically the CPG is performed on the rotated quadrature, \hat{x} . In our case, however, if we were to apply the CPG along \hat{x} and then perform homodyne detection along the same axis, this would amount to an overall phase in the wavefunction and thus would be equivalent to doing just homodyne detection. For details of the derivation, we refer the reader to App. F.

The stellar rank of the associated measurement operators,

$$dx \hat{\Pi}_\gamma = e^{-i\gamma\hat{p}^3} |x\rangle \langle x| e^{i\gamma\hat{p}^3}, \quad (49)$$

is $r^*(\hat{\Pi}_\gamma) = \infty$. This can be inferred from the presence of an Airy function, which contains infinitely many zeroes, in the stellar function. We plot the performance of the CPG in Fig. 3. We find that for increasing cubicity, γ , the error rate degrades. Thus, infinite stellar rank is also not enough to ensure improved performance in BPSK beyond the Gaussian limit.

The stellar rank thus gives us a primitive way to characterise the non-Gaussianity needed for near-optimal BPSK. Under certain circumstances it can provide some criteria for distinguishing some continuously labelled measurement types from e.g. on-off photon detection, something that would be undetectable by Wigner negativity. It does not, however, provide a complete quantification. Although currently lacking, a non-Gaussian resource monotone which is able to do this, as well as inheriting a structure like the stellar hierarchy, would be important for studying non-Gaussianity in more general quantum information contexts.

VII. CONCLUSION

We have explored continuously labelled non-Gaussian operations that minimise the error in discriminating two optical coherent states. This is the first proposal which theoretically allows discrimination beyond the Gaussian limit without using photon detection. We have considered two conceptually different receivers based on non-Gaussian unitaries combined with homodyne detection and orthogonal polynomials.

The first class of receivers were found to be near-optimal for large ranges of the signal state energy $|\alpha|^2$, for three distinct subclasses of receiver, based on rotations by cat states, coherent states, and Fock states. The second class of receivers were also found to be near-optimal for larger ranges of the signal state energy, for two distinct

subclasses, based on the Legendre and Laguerre polynomials. Moreover, all near-optimal receivers we constructed were able to beat the Kennedy receiver limit for significant energy ranges.

Our schemes involving a finite number of rotations by specific classes of states were unable to saturate the Helstrom bound, and it remains an open problem if purely continuously labelled measurements can achieve this. Moreover, techniques for arbitrary gate synthesis in continuous-variable systems may make the creation of such gates possible, paving the way towards a practical realisation [45, 46]. It is also interesting to consider the $N \rightarrow \infty$ limit of Eq. (26). Clearly the optimisation problem over an infinite number of parameters would not be a practical task to solve, but perhaps some insight on whether the measurement scheme can theoretically achieve the Helstrom bound could be uncovered. If this were possible to prove, it would also prove that continuously labelled measurements are sufficient for saturating the Helstrom bound in coherent state discrimination.

The scheme based on the Legendre polynomials performed commensurably with the receivers based on non-Gaussian rotations and homodyne detection in the high-energy limit. The generalised polynomial schemes may offer some insight into the mechanisms of continuously labelled non-Gaussian measurements. We considered only some of the classical orthogonal polynomials but there is a vast literature on generalised orthogonal polynomials such as those organised by the Askey scheme and their q -analogues [47], some of which may have mathematical utility in quantum information tasks, like state discrimination. If they turn out to be of theoretical importance, perhaps further study on their physical realisation may be of interest. We provided a rudimentary quantification of the non-Gaussianity of our receivers as well as known receivers and found that the picture is still unclear. Broadly speaking, designing a measure of non-Gaussianity for quantum measurements that not only provides a resource monotone but can also differentiate between all discretely and continuously labelled measurements might help one understand the limitations of both types of measurement.

The schemes we developed are near-optimal for coherent states. For the discrimination of two arbitrary Gaussian states, an optimal scheme (outside of the projective Helstrom measurement) is still unknown [48, 49]. It may be useful to compare our scheme for discriminating more general Gaussian states with other currently known near-optimal schemes [50, 51]. Moreover, as it was shown that heterodyne detection is optimal amongst Gaussian measurements for quadrature phase-shift keying [28, 29], it could then be worth revisiting the use of the receivers we described here in this context.

Lastly, we may also consider schemes which use additional resources to lower error rates. Allowing access to additional copies of the signal states will always allow one to improve error rates. Moreover, recent schemes involving indefinite causal order (which themselves require

ancillary systems) were shown to improve discrimination probabilities, even when compared with multiple-copy discrimination [52]. Though these results were shown in a purely discrete-variable setting, there exist demonstrations of this phenomenon in hybrid settings [53, 54]. These may allow one to offload complex non-Gaussian operations on the continuous-variable part of the system onto operations on an ancilla system, thereby leveraging the higher efficiency of homodyne detection while also claiming non-Gaussian advantages that typically come from lower-efficiency photon-number measurements.

ACKNOWLEDGMENTS

J.M., S.K., and H.K. are supported by KIAS individual grant numbers QP088701 (J.M.), CG086201 (S.K.), and CG085301 (H.K.) at the Korea Institute for Advanced Study. This work was supported by the Institute of Information & Communications Technology Planning & Evaluation (IITP) grant, funded by the Korean government (MSIT) (No. 2022-0-00463).

Appendix A: Inequivalence of photon detection and homodyne and heterodyne detection

Here we prove the inequivalence of photon detection and homodyne and heterodyne detection. We will show the following:

$$\int_{\psi \in \mathcal{R}} d\psi \mu(\psi) |\psi\rangle \langle \psi| \neq |0\rangle \langle 0| = \sum_{n=0}^{\infty} \sum_{m=0}^{\infty} \delta_{nm} \delta_{n0} |n\rangle \langle m|, \quad (\text{A1})$$

for the instances where $|\psi\rangle = |x\rangle, x \in \mathbb{R}, \mu(\psi) = 1$ a quadrature eigenstate, and $|\psi\rangle = |\beta\rangle, \beta \in \mathbb{C}, \mu(\psi) = \frac{1}{\pi}$, a coherent state. The left-hand side of (A1) may be expanded in diagonal and off-diagonal parts as

$$\begin{aligned} & \int_{\psi \in \mathcal{R}} d\psi \mu(\psi) |\psi\rangle \langle \psi| \\ &= \int_{\psi \in \mathcal{R}} d\psi \mu(\psi) \sum_{n=0}^{\infty} \sum_{m=0}^{\infty} \langle n|\psi\rangle \langle \psi|m\rangle |n\rangle \langle m| \\ &= \int_{\psi \in \mathcal{R}} d\psi \mu(\psi) \sum_{n=0}^{\infty} |\langle n|\psi\rangle|^2 |n\rangle \langle n| + \text{off-diagonal} \\ &= \sum_{n=0}^{\infty} \mathcal{I}_{nn} + \text{off-diagonal}, \end{aligned} \quad (\text{A2})$$

where

$$\mathcal{I}_{nn} = \int_{\psi \in \mathcal{R}} d\psi \mu(\psi) |\langle n|\psi\rangle|^2 |n\rangle \langle n|. \quad (\text{A3})$$

1. Homodyne detection

Firstly, consider $|\psi\rangle = |x\rangle$, a quadrature eigenstate. For any $\mathcal{R} \subseteq \mathbb{R}$, its diagonal elements (A3) are given by

$$\mathcal{I}_{nn} = \left(\frac{1}{\pi}\right)^{\frac{1}{2}} \int_{x \in \mathcal{R}} dx \frac{1}{2^n n!} e^{-x^2} H_n^2(x) |n\rangle \langle n|. \quad (\text{A4})$$

Here we see that the integrand of (A4) is an even function and is positive $\forall x$, meaning we can upper-bound by a larger integration region $\tilde{\mathcal{R}}$ containing \mathcal{R} , such that

$$\tilde{\mathcal{I}}_{nn} = \left(\frac{1}{\pi}\right)^{\frac{1}{2}} \int_{x \in \tilde{\mathcal{R}}} dx \frac{1}{2^n n!} e^{-x^2} H_n^2(x) |n\rangle \langle n|, \quad (\text{A5})$$

and

$$\langle n|\mathcal{I}_{nn}|n\rangle \leq \langle n|\tilde{\mathcal{I}}_{nn}|n\rangle \leq \langle n|\delta_{nn}|n\rangle, \quad (\text{A6})$$

corresponding to the integration regions $\mathcal{R} \subseteq \tilde{\mathcal{R}} \subseteq \mathbb{R}$, where the right-hand side of (A6) comes from the orthogonality relations of the Hermite polynomials, i.e., the integration region $x \in \mathbb{R}$. We see that in order to get a unit projection onto the ground state $\langle 0|\mathcal{I}_{00}|0\rangle$ we need to take the set $\mathcal{R} = \mathbb{R}$, i.e. the resolution of the identity for the quadrature eigenstates. Thus we conclude that vacuum state projection is not possible by any splitting of integration regions in homodyne detection.

2. Heterodyne detection

Next we consider $|\psi\rangle = |\beta\rangle$. The diagonal elements (A3) in radial coordinates are

$$\mathcal{I}_{nn} = 2 \int_{r \in \mathcal{R}} dr \frac{r^{1+2n} e^{-r^2}}{n!} |n\rangle \langle n|. \quad (\text{A7})$$

Given that there is no explicit angular dependence in the integral and the integrand is positive on $r \in [0, \infty)$, we may circle the region \mathcal{R} by a larger region $\tilde{\mathcal{R}}$ containing \mathcal{R} and the same chain of inequalities as (A6) follows with unit projection onto the vacuum state this time only being possible with $\mathcal{R} = \mathbb{C}$, which just recovers the completeness relation for the coherent states. Thus no splitting of integration regions in heterodyne detection can reproduce on-off photon detection.

Appendix B: Rotating by Fock states with increasing N

Consider the unitary operator Eq. (25) with Fock states,

$$\{|\psi_k\rangle\} = \{|k\rangle\}, \quad (\text{B1})$$

In order to obtain some concrete results we perform a numerical optimisation for various N , showing that increasing N can improve the error rate of receivers based

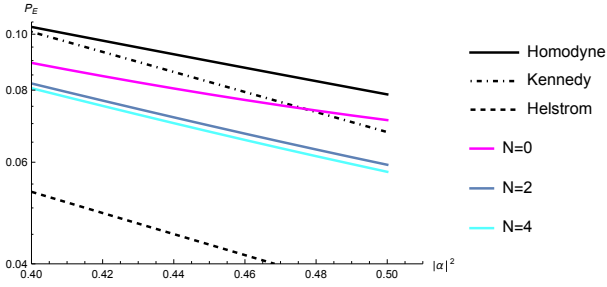


FIG. 4. Error rates for Fock state rotation based receivers, $\hat{\Pi}_{\{|k\rangle\}}^{(N)}$, for different values of N with $|\mathcal{S}_1| = 1$, $|\mathcal{S}_2| = 3$, and $|\mathcal{S}_3| = 5$ corresponding to the sets in (B2). We find that the error rate decreases with increasing N .

on unitary rotations by pure state projectors as described in Sec. IV A. Though these receivers allow us to enter the near-optimal regime, they are ultimately outperformed by other continuously labelled receivers considered in Tab. I.

We know that the performance of a receiver with N rotations can at worst be equal to the performance of a receiver with $N - 1$ rotations, because the rotation angle of the N^{th} may always be set to $\theta_N = 0$. Here we show an explicit example. Consider the following three cases:

$$\begin{aligned} \mathcal{S}_1 &= \{|1\rangle\}, \\ \mathcal{S}_2 &= \{|0\rangle, |1\rangle, |2\rangle\}, \\ \mathcal{S}_3 &= \{|0\rangle, |1\rangle, |2\rangle, |3\rangle, |4\rangle\}, \end{aligned} \quad (\text{B2})$$

where the optimal rotation angles, $\vec{\theta}_{\mathcal{S}_i}(\alpha)$, are determined numerically. Over the range of $|\alpha|^2$ considered, we observe that $\vec{\theta}_{\mathcal{S}_1}(\alpha) = (\pi)$, $\vec{\theta}_{\mathcal{S}_2}(\alpha) = (\pi, \pi, \pi)$, and $\vec{\theta}_{\mathcal{S}_3}(\alpha)$ is variable. Their respective error rates are plotted in Fig. 4. The error rates decrease with increasing N and as such we conclude that increasing N can improve performance.

Appendix C: Optimal parameters for coherent state and cat state rotations

Here we show that the cat and coherent state parameters, β , follow an approximately linear scaling in the coherent state intensity. In Fig. 5 we plot the optimal values of β for both the coherent state and cat state rotations as a function of $|\alpha|^2$, with a spacing between points of $\Delta|\alpha|^2 = 0.01$. Over the energy ranges consider in the paper, $0 < |\alpha| \leq 3$, we found that a linear fit on the coherent states has a scaling of $1.07 + 0.296|\alpha|^2$ and the cat states have a fit of $0.715 + 0.355|\alpha|^2$. We remark that the linear fit is more accurate for the coherent state rotations. Note that we exclude the point $|\alpha|^2 = 0$ because this corresponds to discriminating two identical vacuum states, for which no unitary preprocessing can help.

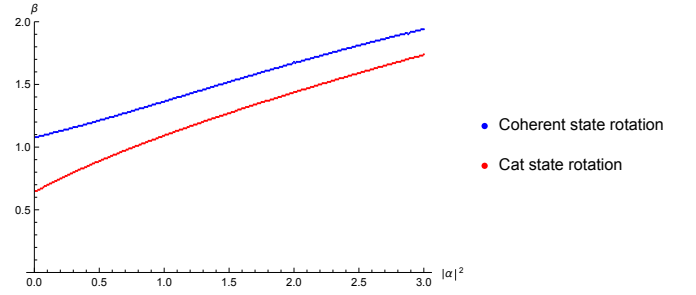


FIG. 5. The optimal values of β for both cat and coherent state rotations, $\hat{\Pi}_{\{|\text{cat}(\beta)\rangle\}}^{(0)}$ and $\hat{\Pi}_{\{|k\rangle\}}^{(N)}$, as a function of the input state intensity, $|\alpha|^2$, for $0.01 \leq |\alpha|^2 \leq 3$.

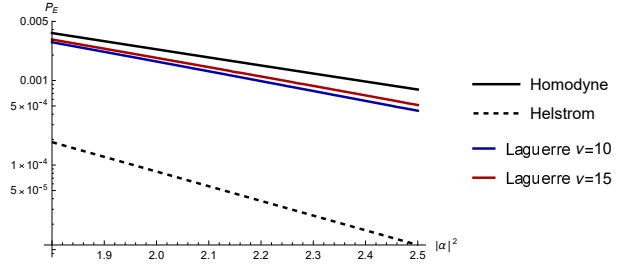


FIG. 6. Performance of the PACS-based receivers $\hat{\Pi}_{\beta;1}$ and $\hat{\Pi}_{\beta;2}$, and CPG-based receivers, $\hat{\Pi}_{\gamma}$, for $\gamma = 0.1$ and $\gamma = 1$ versus homodyne detection.

Appendix D: Orthogonal polynomial states

Classical orthogonal polynomials, $P_n(\psi)$, satisfy the following orthogonality conditions

$$\int_{\psi \in \mathcal{X}} d\psi w(\psi) P_n(\psi) P_m(\psi) = \delta_{nm}, \quad (\text{D1})$$

where $w(\psi)$ is some positive weight function. There are three distinct families of classical orthogonal polynomials, these are: the Hermite polynomials, orthogonal on $\mathcal{X} = \mathbb{R}$; the Laguerre polynomials, orthogonal on $\mathcal{X} = [0, \infty)$; and the Jacobi polynomials, orthogonal on $\mathcal{X} = [-1, 1]$ [47, 55]. The essential properties of the three families of classical orthogonal polynomials are summarised in Tab. II.

Property (D1) allows us to construct generalised quantum states,

$$|\psi\rangle = \frac{1}{\sqrt{w(\psi)}} \sum_{n=0}^{\infty} P_n(\psi) |n\rangle, \quad (\text{D2})$$

which satisfy the completeness relation

$$\int_{\psi \in \mathcal{X}} d\psi |\psi\rangle \langle \psi| = \sum_{n=0}^{\infty} |n\rangle \langle n| = \mathbb{I}. \quad (\text{D3})$$

When we choose the Hermite polynomials, the generalised quantum states (D2) become the quadrature

TABLE II. Classical orthogonal polynomials, their Rodrigues' formulas, and their weight functions. The generalised Laguerre and Jacobi polynomials come with additional parameters satisfying $\nu, \mu > -1$.

Polynomial	$P_n(x)$	$w(x)$
Hermite $H_n(x)$	$(-1)^n e^{x^2} \frac{d^n}{dx^2} e^{-x^2}$	e^{-x^2}
Laguerre $L_n^{(\nu)}(x)$	$\frac{x^{-\nu}}{n!} \left(\frac{d}{dx} - 1 \right)^n x^{n+\nu}$	$\frac{n! x^\nu e^{-x}}{\Gamma(n+\nu+1)}$
Jacobi $J_n^{(\nu, \mu)}(x)$	$\frac{(-1)^n (1-x)^{-\nu} (1+x)^{-\mu}}{2^n n!} \frac{d^n}{dx^n} \left((1-x)^\nu (1+x)^\mu (1-x^2)^n \right)$	$\frac{(1-x)^\nu (1+x)^\mu (2n+\nu+\mu+1) \Gamma(n+\nu+\mu+1) n!}{2^{\nu+\mu+1} \Gamma(n+\nu+1) \Gamma(n+\mu+1)}$

eigenstates and these also define the Gaussian limit for BPSK. If the generalised Laguerre polynomials are chosen, the generalised quantum states resemble Laguerre-Gauss modes [56, 57], up to a rescaling of the radial variable. We found a very slight non-Gaussian advantage using these states as mentioned in Tab. I. When the Jacobi polynomial states are chosen, these do not appear in the literature, perhaps because a variable constrained to the interval $[-1, 1]$ lacks an obvious physical interpretation. Nevertheless, we can define measurements with these states, and when the parameters $\nu = \mu = 0$, the Jacobi polynomials are precisely the Legendre polynomials studied in the main text in Sec. V.

Given the improvement beyond the Gaussian limit, we know that the generalised polynomial states have non-Gaussian character, though determining their stellar rank involves counting the zeroes of the series

$$F_P^*(\alpha) = \frac{1}{\sqrt{w(\psi)}} \sum_{n=0}^{\infty} \frac{P_n(\psi)}{\sqrt{n!}} \alpha^n, \quad (\text{D4})$$

which for the Laguerre and Jacobi polynomials seems difficult to do. We know, however, given the observed non-Gaussian improvement, these series must have at least one zero.

In Fig. 6 we plot the error rate for a receiver based on generalised Laguerre polynomials for the parameters $\nu = 10$ and $\nu = 15$. We observe a slight improvement over the homodyne limit, verifying their non-Gaussian character, but the improvement is only marginal.

Appendix E: Stellar rank and photon-added coherent states

Here we briefly introduce the stellar rank and the stellar hierarchy of non-Gaussian states. Described in [37], the stellar function for a pure state in an infinite-dimensional Hilbert space is defined by

$$F_\psi^*(\alpha) = e^{\frac{1}{2}|\alpha|^2} \langle \alpha^* | \psi \rangle = \sum_{n \geq 0} \psi_n \frac{\alpha^n}{\sqrt{n!}}, \quad \forall \alpha \in \mathbb{C}, \quad (\text{E1})$$

which is closely related to the Husimi Q-distribution [58, 59] through

$$Q_\psi(\alpha) = \frac{1}{\pi} |\langle \alpha | \psi \rangle|^2 = \frac{e^{-|\alpha|^2}}{\pi} |F_\psi^*(\alpha)|^2. \quad (\text{E2})$$

The stellar rank, $r^*(\psi)$, thus organises non-Gaussian states by partitioning the infinite-dimensional Hilbert space of states into classes with the same number of zeroes in their stellar functions. Any pure state may then be expressed as [37]

$$|\psi\rangle = F_\psi^*(\hat{a}^\dagger) |0\rangle. \quad (\text{E3})$$

For a state of finite stellar rank we have the following

$$|\psi\rangle = \frac{1}{\mathcal{N}} \left[\prod_{n=1}^{r^*(\psi)} \hat{D}(\beta_n) a^\dagger \hat{D}^\dagger(\beta_n) \right] |G_\psi\rangle. \quad (\text{E4})$$

Here $|G_\psi\rangle$ is a reference Gaussian state and \mathcal{N} is a normalisation. This decomposition is unique up to a reordering of the roots. We see that the stellar rank essentially counts the number of photon-additions needed to create the state $|\psi\rangle$ from a reference Gaussian state. It thus provides a hierarchy of non-Gaussian states.

For n-PACS we can immediately determine their stellar rank by rewriting Eq. (45) as

$$|\beta; n\rangle = \frac{1}{\sqrt{n!}} \prod_{i=1}^n \left[\hat{D}(\beta) a^\dagger \hat{D}^\dagger(\beta) \right] |\beta\rangle, \quad (\text{E5})$$

thus we have $r^*(\hat{\Pi}_{\beta;n}) = n$, and their completeness relation is given by

$$\int_{\beta \in \mathbb{C}} \frac{d^2\beta}{\pi} |\beta; n\rangle \langle \beta; n| = \mathbb{I}, \quad (\text{E6})$$

which is valid $\forall n$.

Appendix F: Cubic phase gate

In order to determine the wavefunction for the cubic phase gate, consider the following

$$\begin{aligned} \langle x | e^{i\gamma \hat{p}^3} | \alpha \rangle &= \langle x | \int_{p \in \mathbb{R}} dp e^{i\gamma p^3} |p\rangle \langle p | \alpha \rangle \\ &= \left(\frac{1}{4\pi^3} \right)^{\frac{1}{4}} \int_{p \in \mathbb{R}} dp e^{ip(x - \sqrt{2}\alpha)} e^{i\gamma p^3} e^{-\frac{1}{2}p^2}, \end{aligned} \quad (\text{F1})$$

where $|p\rangle$ is a momentum eigenstate. By using results contained in [60], in particular, the following identity:

$$\begin{aligned} & \int_{y \in \mathbb{R}} dy \exp\left(ixy - \frac{1}{2}y^2 + \frac{i}{3}\gamma y^3\right) \\ &= 2\pi|\gamma|^{-\frac{1}{3}} \exp\left(\frac{1}{12\gamma^2} + \frac{x}{2\gamma}\right) \text{Ai}\left(\gamma^{-\frac{1}{3}}\left(x + \frac{1}{4\gamma}\right)\right), \end{aligned} \quad (\text{F2})$$

we find that the wavefunction (F1) is then equal to

$$\begin{aligned} \langle x | e^{i\gamma \hat{p}^3} | \alpha \rangle = \\ \frac{(4\pi)^{\frac{1}{4}}}{|3\gamma|^{\frac{1}{3}}} e^{\frac{1}{108\gamma^2}} e^{\frac{x-\sqrt{2}\alpha}{6\gamma}} \text{Ai}\left((3\gamma)^{-\frac{1}{3}}\left(x - \sqrt{2}\alpha + \frac{1}{12\gamma}\right)\right). \end{aligned} \quad (\text{F3})$$

- Recovering the wavefunction quoted in the main text.
-
- [1] S. M. Barnett and S. Croke, Quantum state discrimination, *Adv. Opt. Photon.* **1**, 238 (2009).
- [2] J. Bae and L.-C. Kwek, Quantum state discrimination and its applications, *J. Phys. A Math. Theor.* **48**, 083001 (2015).
- [3] M. A. Nielsen and I. L. Chuang, *Quantum Computation and Quantum Information: 10th Anniversary Edition* (Cambridge University Press, 2011).
- [4] S. Pirandola, U. L. Andersen, L. Banchi, M. Berta, D. Bunandar, R. Colbeck, D. Englund, T. Gehring, C. Lupo, C. Ottaviani, J. L. Pereira, M. Razavi, J. S. Shaari, M. Tomamichel, V. C. Usenko, G. Vallone, P. Villoresi, and P. Wallden, Advances in quantum cryptography, *Adv. Opt. Photon.* **12**, 1012 (2020).
- [5] J. S. Sidhu, S. K. Joshi, M. Gündoğan, T. Brougham, D. Lowndes, L. Mazzarella, M. Krutzik, S. Mohapatra, D. Dequal, G. Vallone, P. Villoresi, A. Ling, T. Jennewein, M. Mohageg, J. G. Rarity, I. Fuentes, S. Pirandola, and D. K. L. Oi, Advances in space quantum communications, *IET Quantum Commun.* **2**, 182 (2021).
- [6] C. W. Helstrom, Quantum detection and estimation theory, *J. Stat. Phys.* **1**, 231 (1969).
- [7] J. Kahn, A. Gnauck, J. Veselka, S. Korotky, and B. Kasper, 4-gb/s psk homodyne transmission system using phase-locked semiconductor lasers, *IEEE Photonics Technology Letters* **2**, 285 (1990).
- [8] C. Wittmann, M. Takeoka, K. N. Cassemiro, M. Sasaki, G. Leuchs, and U. L. Andersen, Demonstration of near-optimal discrimination of optical coherent states, *Phys. Rev. Lett.* **101**, 210501 (2008).
- [9] M. Takeoka and M. Sasaki, Discrimination of the binary coherent signal: Gaussian-operation limit and simple non-gaussian near-optimal receivers, *Phys. Rev. A* **78**, 022320 (2008).
- [10] R. Han, J. A. Bergou, and G. Leuchs, Near optimal discrimination of binary coherent signals via atom-light interaction, *New J. Phys.* **20**, 043005 (2018).
- [11] J. S. Sidhu, M. S. Bullock, S. Guha, and C. Lupo, Linear optics and photodetection achieve near-optimal unambiguous coherent state discrimination, *Quantum* **7**, 1025 (2023).
- [12] S. J. Dolinar, An optimum receiver for the binary coherent state quantum channel, *MIT Res. Lab. Elec. Q. Prog. Rep.* **111**, 115 (1973).
- [13] M. Sasaki and O. Hirota, Optimum decision scheme with a unitary control process for binary quantum-state signals, *Phys. Rev. A* **54**, 2728 (1996).
- [14] R. J. Glauber, The quantum theory of optical coherence, *Phys. Rev.* **130**, 2529 (1963).
- [15] E. C. G. Sudarshan, Equivalence of semiclassical and quantum mechanical descriptions of statistical light beams, *Phys. Rev. Lett.* **10**, 277 (1963).
- [16] C. Weedbrook, S. Pirandola, R. García-Patrón, N. J. Cerf, T. C. Ralph, J. H. Shapiro, and S. Lloyd, Gaussian quantum information, *Rev. Mod. Phys.* **84**, 621 (2012).
- [17] G. Adesso, S. Ragy, and A. R. Lee, Continuous variable quantum information: Gaussian states and beyond, *Open Syst. Inf. Dyn.* **21**, 1440001 (2014).
- [18] M. Walschaers, Non-gaussian quantum states and where to find them, *PRX Quantum* **2**, 030204 (2021).
- [19] G. Giedke and J. Ignacio Cirac, Characterization of gaussian operations and distillation of gaussian states, *Phys. Rev. A* **66**, 032316 (2002).
- [20] I. B. Djordjevic, *Quantum Communication, Quantum Networks, and Quantum Sensing Book* (Academic Press, 2022).
- [21] D. Walls and G. J. Milburn, *Quantum Optics* (Springer Berlin, Heidelberg, 2008).
- [22] D. E. Roberson, S. Izumi, W. Roga, J. S. Neergaard-Nielsen, M. Takeoka, and U. L. Andersen, Limit of gaussian operations and measurements for gaussian state discrimination and its application to state comparison, *Phys. Rev. A* **103**, 022423 (2021).
- [23] S. Izumi, M. Takeoka, K. Wakui, M. Fujiwara, K. Ema, and M. Sasaki, Projective measurement onto arbitrary superposition of weak coherent state bases, *Sci. Rep.* **8**, 2999 (2018).
- [24] R. L. Cook, P. J. Martin, and J. M. Geremia, Optical coherent state discrimination using a closed-loop quantum measurement, *Nature* **446**, 774 (2007).
- [25] R. S. Kennedy, A near-optimum receiver for the binary coherent state quantum channel, *Quart. Prog. Rep.* **108** (1973).
- [26] J. Geremia, Distinguishing between optical coherent states with imperfect detection, *Phys. Rev. A* **70**, 062303 (2004).
- [27] A. Assalini, N. Dalla Pozza, and G. Pierobon, Revisiting the dolinar receiver through multiple-copy state discrim-

- ination theory, *Phys. Rev. A* **84**, 022342 (2011).
- [28] S. Yamazaki and K. Emura, Feasibility study on qpsk optical-heterodyne detection system, *J. Light. Technol.* **8**, 1646 (1990).
- [29] C. R. Müller, M. A. Usuga, C. Wittmann, M. Takeoka, C. Marquardt, U. L. Andersen, and G. Leuchs, Quadrature phase shift keying coherent state discrimination via a hybrid receiver, *New J. Phys.* **14**, 083009 (2012).
- [30] B.-G. Englert, Fringe visibility and which-way information: An inequality, *Phys. Rev. Lett.* **77**, 2154 (1996).
- [31] A. Aiello, A probabilistic view of wave-particle duality for single photons, *Quantum* **7**, 1135 (2023).
- [32] S. L. Braunstein and P. van Loock, Quantum information with continuous variables, *Rev. Mod. Phys.* **77**, 513 (2005).
- [33] M. Munroe, D. Boggavarapu, M. E. Anderson, and M. G. Raymer, Photon-number statistics from the phase-averaged quadrature-field distribution: Theory and ultrafast measurement, *Phys. Rev. A* **52**, R924 (1995).
- [34] F. Albarelli, M. G. Genoni, M. G. A. Paris, and A. Ferraro, Resource theory of quantum non-gaussianity and wigner negativity, *Phys. Rev. A* **98**, 052350 (2018).
- [35] J. Park, J. Lee, K. Baek, S.-W. Ji, and H. Nha, Faithful measure of quantum non-gaussianity via quantum relative entropy, *Phys. Rev. A* **100**, 012333 (2019).
- [36] B. Regula, L. Lami, G. Ferrari, and R. Takagi, Operational quantification of continuous-variable quantum resources, *Phys. Rev. Lett.* **126**, 110403 (2021).
- [37] U. Chabaud, D. Markham, and F. Grosshans, Stellar representation of non-gaussian quantum states, *Phys. Rev. Lett.* **124**, 063605 (2020).
- [38] G. S. Agarwal and K. Tara, Nonclassical properties of states generated by the excitations on a coherent state, *Phys. Rev. A* **43**, 492 (1991).
- [39] G. S. Agarwal and K. Tara, Nonclassical character of states exhibiting no squeezing or sub-poissonian statistics, *Phys. Rev. A* **46**, 485 (1992).
- [40] N. Budinger, A. Furusawa, and P. van Loock, All-optical quantum computing using cubic phase gates, *Phys. Rev. Res.* **6**, 023332 (2024).
- [41] A. Sakaguchi, S. Konno, F. Hanamura, W. Asavanant, K. Takase, H. Ogawa, P. Marek, R. Filip, J.-i. Yoshikawa, E. Huntington, H. Yonezawa, and A. Furusawa, Nonlinear feedforward enabling quantum computation, *Nat. Commun.* **14**, 3817 (2023).
- [42] K. Miyata, H. Ogawa, P. Marek, R. Filip, H. Yonezawa, J.-i. Yoshikawa, and A. Furusawa, Implementation of a quantum cubic gate by an adaptive non-gaussian measurement, *Phys. Rev. A* **93**, 022301 (2016).
- [43] S. Konno, W. Asavanant, K. Fukui, A. Sakaguchi, F. Hanamura, P. Marek, R. Filip, J.-i. Yoshikawa, and A. Furusawa, Non-clifford gate on optical qubits by nonlinear feedforward, *Phys. Rev. Res.* **3**, 043026 (2021).
- [44] M. Abramowitz and I. A. Stegun, eds., *Handbook of Mathematical Functions with Formulas, Graphs and Mathematical Tables* (Dover Publications, Inc., 1965).
- [45] J. M. Arrazola, T. R. Bromley, J. Izaac, C. R. Myers, K. Brádler, and N. Killoran, Machine learning method for state preparation and gate synthesis on photonic quantum computers, *QST* **4**, 024004 (2019).
- [46] T. Kalajdzievski and N. Quesada, Exact and approximate continuous-variable gate decompositions, *Quantum* **5**, 394 (2021).
- [47] R. Koekoek and R. F. Swarttouw, The askey-scheme of hypergeometric orthogonal polynomials and its q-analogue, arXiv:9602214 (1996).
- [48] S. Olivares and M. G. A. Paris, Binary optical communication in single-mode and entangled quantum noisy channels, *J. Opt. B: Quantum Semiclass. Opt.* **6**, 69 (2004).
- [49] G. Cariolaro and G. Pierobon, Performance of quantum data transmission systems in the presence of thermal noise, *IEEE Trans. Commun.* **58**, 623 (2010).
- [50] M. N. Notarnicola, M. G. A. Paris, and S. Olivares, Hybrid near-optimum binary receiver with realistic photon-number-resolving detectors, *J. Opt. Soc. Am. B* **40**, 705 (2023).
- [51] D. Sych and G. Leuchs, Practical receiver for optimal discrimination of binary coherent signals, *Phys. Rev. Lett.* **117**, 200501 (2016).
- [52] S. Kechrimparis, J. Moran, A. Karsa, C. Lee, and H. Kwon, Enhancing quantum state discrimination with indefinite causal order, arXiv:2406.19373 (2024).
- [53] H. C. J. Gan, G. Maslennikov, K.-W. Tseng, C. Nguyen, and D. Matsukevich, Hybrid quantum computing with conditional beam splitter gate in trapped ion system, *Phys. Rev. Lett.* **124**, 170502 (2020).
- [54] P. Yin, X. Zhao, Y. Yang, Y. Guo, W.-H. Zhang, G.-C. Li, Y.-J. Han, B.-H. Liu, J.-S. Xu, G. Chiribella, G. Chen, C.-F. Li, and G.-C. Guo, Experimental superheisenberg quantum metrology with indefinite gate order, *Nat. Phys.* **19**, 1122 (2023).
- [55] G. Szegő, *Orthogonal Polynomials* (American Mathematical Society, 1975).
- [56] N. B. Simpson, K. Dholakia, L. Allen, and M. J. Padgett, Mechanical equivalence of spin and orbital angular momentum of light: an optical spanner, *Opt. Lett.* **22**, 52 (1997).
- [57] A. T. O'Neil, I. MacVicar, L. Allen, and M. J. Padgett, Intrinsic and extrinsic nature of the orbital angular momentum of a light beam, *Phys. Rev. Lett.* **88**, 053601 (2002).
- [58] K. Husimi, Some formal properties of the density matrix, *Proc. Phys. Math. Soc. Jpn.* **22**, 264 (1940).
- [59] K. E. Cahill and R. J. Glauber, Density operators and quasiprobability distributions, *Phys. Rev.* **177**, 1882 (1969).
- [60] M. Brunelli and O. Houhou, Linear and quadratic reservoir engineering of non-gaussian states, *Phys. Rev. A* **100**, 013831 (2019).